Journal of Manufacturing Processes 57 (2020) 828–846

Contents lists available at ScienceDirect

Journal of Manufacturing Processes

journal homepage: www.elsevier.com/locate/manpro

A process control and interlayer heating approach to reuse polyamide 12 powders and create parts with improved mechanical properties in selective laser sintering

Feifei Yang[a], Tianyu Jiang[a], Greg Lalier[b], John Bartolone[b], Xu Chen[a,*]

[a] Department of Mechanical Engineering, University of Washington, Seattle, WA, 98195, USA
[b] Unilever Research & Development, 45 Commerce Drive, Trumbull, CT, 06611, USA

ARTICLE INFO

Keywords:
Selective laser sintering
Powder reuse
Powder aging and degradation
Interlayer heating
Sustainability

ABSTRACT

Capable of building high-quality, complex parts directly from digital models, selective laser sintering (SLS) additive manufacture (AM) is a core method of agile manufacturing. Polyamide 12 is the most commonly and successfully used polymer powders to date in SLS due to the conforming thermal behaviors of this thermoplastic polymer. State of the art technology produces a substantial amount of un-sintered powders after the manufacturing process. Failure to recycle and reuse these aged powders not only leads to economic losses but also is environmentally unfriendly. This is particularly problematic for powders close to the heat-affected zones that go through severe thermal degradations during the laser sintering processes. Limited procedures exist for systematically reusing such extremely aged powders. This work proposes a new process control method to maximize reusability of aged and extremely aged polyamide 12 powders. Building on a previously untapped interlayer heating, preprocessing, and mixing of powder materials, we show how reclaimed polyamide 12 powders can be consistently reprinted into functional samples, with mechanical properties even superior to current industrial norms. In particular, the proposed method can yield printed samples with 18.04 % higher tensile strength and 55.29 % larger elongation at break using as much as 30 % of extremely aged powders compared to the benchmark sample.

1. Introduction

Capable of processing almost any laser-absorbent materials including polymers, metals, ceramics and composites, selective laser sintering (SLS) is one of the most well established and commonly used additive manufacturing (AM) techniques to rapidly manufacture three-dimensional components [1–4]. Polymeric powders, semicrystalline or amorphous, are the first and still the most widely applied materials in SLS [1,5,6]. Parts printed using amorphous polymer powders are partially consolidated, and consequently can be useful for applications when the strength and durability of parts are not dominant [7]. On the contrary, parts printed using semicrystalline polymer powders are fully consolidated with high mechanical strength and effectively weakened warpage. Among the semicrystalline polymers, polyamide families are the most popular for SLS, and polyamide 12 dominates the market because of the capability to generate strong parts for common applications [3,4,8]. To be more specific, parts printed using polyamide 12 powders have superior mechanical properties than that of parts from amorphous polymers. The superior mechanical properties originate from the thermal behaviors of the semicrystalline materials [9–11], including, e.g., a wide processing window for sintering, high melting enthalpy, and high flowability [3,12]. The existence of a wide sintering window between melting onset and crystallization onset temperatures is beneficial for maximizing part consolidation to get a fully dense part [13]. High melting enthalpy and high flowability are necessary during laser sintering to get a homogeneous powder layer and to melt the powder locally with high accuracy and reproducibility [2,12].

Despite the popular applications of the polyamide 12 powders in SLS, the volume ratio of powders that translate to parts is small: e.g., commonly 5 %–15 % of the total powders in the build chamber. The 85 %–95 % residual powders went through deteriorate physical and chemical degradations in the intricate fabricating processes including preheating, sintering, cooling, and/or post treatment [3,14], but have the potential to be recycled and reused for further applications

* Corresponding author.
E-mail addresses: yangff@uw.edu (F. Yang), tjiang19@uw.edu (T. Jiang), Greg.Lalier@unilever.com (G. Lalier), John.Bartolone@unilever.com (J. Bartolone), chx@uw.edu (X. Chen).

https://doi.org/10.1016/j.jmapro.2020.07.051
Received 11 February 2020; Received in revised form 23 July 2020; Accepted 27 July 2020

[3,4,15,16]. However, the deteriorated powders have reduced surface morphologies, larger and more complex molecular chains, decreased flowability, and deteriorated mechanical and thermal properties, which make it challenging to reuse them directly [3,4,13,15,16]. Also, polyamide 12 powder is relatively expensive, priced around $150/kg in 2019 [14]. Abandonment of the residual polyamide 12 powders can cause not only economic losses but also environmental pollution. Thus, reclaim and reuse are difficult yet necessary for a sustainable SLS AM.

Prior to reuse, characterizations, such as powder flowability, melt volume rate (MVR) and viscosity, are studied to exhibit the differences between polyamide 12 new powders and reclaimed powders. Sufficient flowability is a necessity in SLS to enable processing of powders and deposition of powder layers [17]. Many efforts have been done to understand the static and dynamic flow behaviors of polyamide 12 powders, and to optimize the flowability [17,18]. Particle shape significantly impacts powder flowability. High sphericity leads to high flowability, potato-shaped particles the next, and rough-edged irregular particles exhibit the lowest flowability [19]. MVR index reveals changing flowability of the powders due to degradation [3,15,20]. New polyamide 12 powders have higher MVR values, while reclaimed powders have lower MVR values [20]. Besides, longer aging or multiple times of reusing lead to smaller MVR values. Reclaimed polyamide 12 powders have increased zero-shear viscosity compared to new powders [3,4]. Moreover, a higher temperature accelerates aging and increases zero-shear viscosity [4]. The increase of zero-shear viscosity for reclaimed powders results from the post-condensation phenomena. It also increases molecular weight of reclaimed polyamide 12 powders, as confirmed by Gel permeation chromatography (GPC) [4].

From there, relevant works on the reuse of the reclaimed polyamide 12 powders have been reported in recent years. L. Feng et al. [14] reclaimed polyamide 12 from SLS and made the powders into filaments for fused deposition modeling (FDM). L. Wang et al. [21] demonstrated a closed-loop recycling of polyamide12 powder from SLS into milled carbon fiber/recycled polyamide 12 composite filaments for extrusion-based AM. The effect of prolonged storage at elevated temperatures on the isothermal crystallization kinetics of polyamide 12 has been studied using Flash Differential Scanning Calorimetry (DSC) experiments by F. Paolucci et al. [12]. Clarifying the aging mechanisms on thermal behavior, coalescence behavior and the resulting crystallinity, microstructure and mechanical properties, and investigating systematic aging mechanisms and microstructural evolution, P. Chen et al. [3] and S. Dadbakhsh et al. [4] characterized the aging process of polyamide 12 powders in SLS. Dotchev et al. [15], Wegner et al. [20] and Josupeit et al. [11] verified the decreased flowability of the reclaimed polyamide 12 powders compared to new ones through a MVR index, which was recommended as a measure of the powder degradation rates. K. Wudy et al. [22,23] investigated the influences of processing time and temperature on aging effects of polyamide 12 in SLS. In particular, the references (i) studied molecular changes and thermal property changes of polyamide 12 partcake material, and (ii) examined the aging behavior of polyamide 12 in SLS including bulk characteristics and part properties such as porosity and surface roughness. The effect of powder reuse on mechanical properties has been studied by R.D. Goodridge et al. [24] and K. Wudy et al. [25], who pointed out the changes of tensile strength as well as elongation at break in parts built from aged polyamide 12 powders. In addition, the relationships between preheating temperature [20], energy density [20,26], combined dwelling time between layers, energy density [27], and part quality were studied.

The complex aging mechanism of polyamide 12 powders in laser-sintering involves a set of physical and chemical processes. The reversible physical degradation here mainly leads to changing molecule order or concentration, particle post-crystallization and agglomeration [20]. The chemical degradation, on the other hand, is irreversible and predominant in the aging process. The chemical degradation changes such polymer structures as chain scission, branching and cross-linking caused by oxidation, post-condensation and hydrolyzes. Previous studies have revealed that thermal oxidation and post-condensation are two main aging mechanisms in chemical degradation during SLS [4,25]. The oxidation process is initiated by free molecule radicals (hydrogen radical) emerging from the decomposition of the polyamide 12. After oxygen addition and transfer, termination reaction occurs to form stable final products (e.g., hydroperoxide and imide groups) and to complete the oxidation reaction. Apart from the thermal oxidation reaction, post-condensation is another irreversible chemical degradation behavior of polyamide 12 that leads to property changes in reclaimed powders [12,25]. Here, the lengths of polymer molecular chain increase through combinations of free radicals at high temperatures. As a result, the molecular weight, flowability and viscosity of the reclaimed polyamide 12 change.

Although existing efforts have sought to understand the aging mechanisms and reuse of the degraded polyamide 12 powders, the possibility and feasibility of reusing the residual polyamide 12 powders remain not fully exploited. In particular, the reuse of the extremely aged polyamide 12 powders closes to the heat-affected zones (HAZs)* has not been reported. This paper seeks to bridge the missing link and proposes a new method, hereby referred to as active interlayer heating, to build parts with the reclaimed and extremely aged polyamide 12 powders. We discuss a new process control approach to reuse the polyamide 12 powders of different degradation levels, different mixing percentages, and different combinations with multiple layer printing and superior mechanical properties. The result is that reclaimed polyamide 12 powders can be consistently reprinted into functional samples, with mechanical properties comparable or even superior to current industrial norms. In particular, the proposed method can yield printed samples with 18.04 % higher tensile strength and 55.29 % larger elongation at break using as much as 30 % of extremely aged powders.

2. Proposed active interlayer heating for reusing aged and extremely aged polyamide 12 powders

Fig. 1 outlines the flowchart of the proposed approach. The main procedures include powder collection, preprocessing, powder mixing, powder characterizations, parameter control, interlayer heating, and part characterizations. Below, we discuss each procedure in detail.

2.1. Materials sample preparation

2.1.1. Powder samples

In this study, we collected polyamide 12 powders purchased from EOS Corp. and reclaimed from standard SLS processes on an EOS P 390 machine. The powders cover three levels of degradation: (i) new powders without heat treatment, (ii) aged powders located far away from the HAZs during SLS and currently reused in the industry, and (iii) extremely aged powders located close to the HAZs and not being actively reused in SLS. Strong laser-material interaction occurs during the sintering process at or close to HAZs, leading to complex aging and degradation of the powder materials. The intricate laser-induced thermophysics change properties of polyamide powders such as particle sizes/shapes, microstructures, thermal properties and mechanical properties. Consequently, extremely aged powders are more severely degraded than the aged powders due to its closer location to the HAZs.

2.1.2. Powder preprocess

Different from new powders and aged powders, extremely aged powders went through severe degradations induced by high temperature and intense laser-material interactions. Consequently, the collected extremely aged powders clump together and suffer from severe aggregation, which adversely impact the powder coating process. As

* Areas close to the laser-material interaction during sintering.

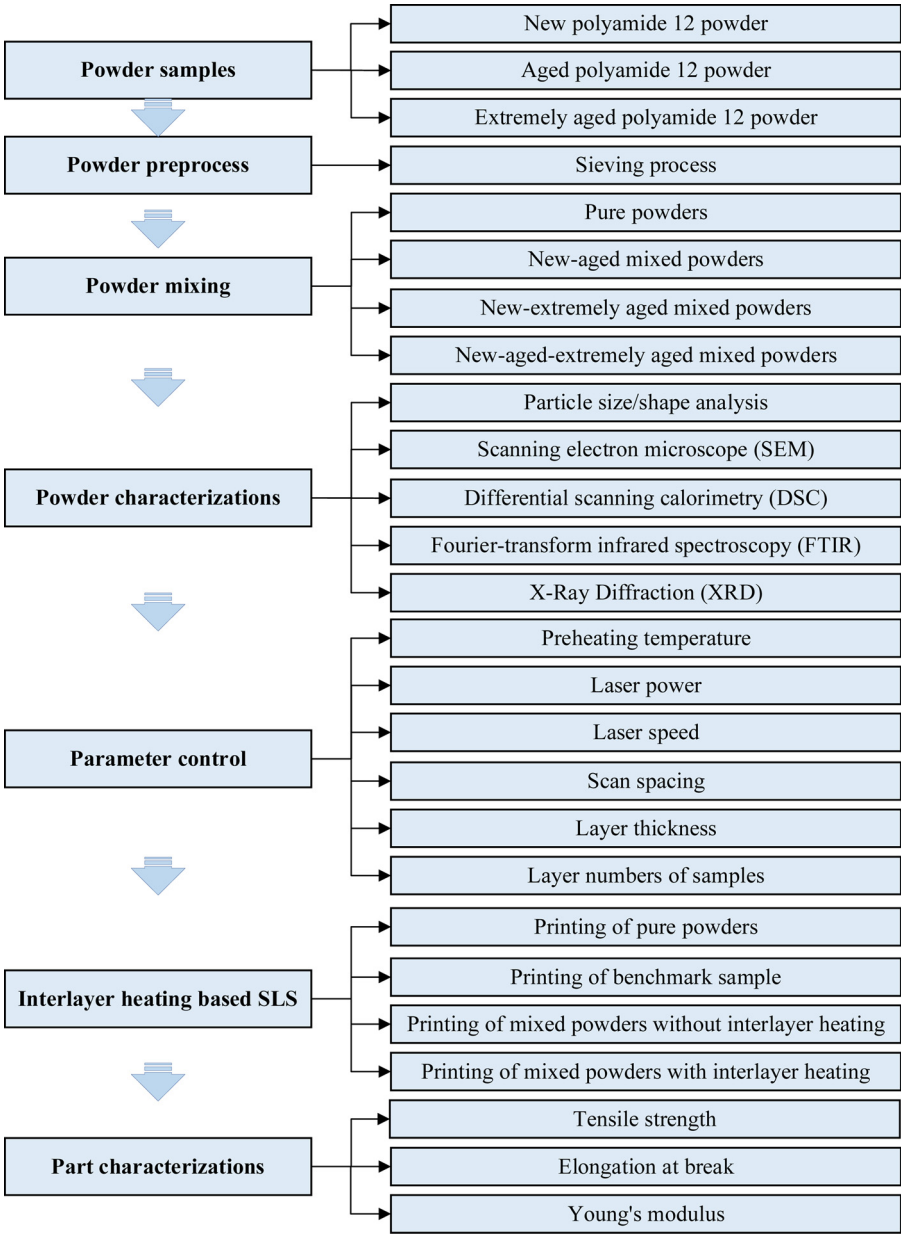

Fig. 1. Proposed method for reusing aged and extremely aged polyamide 12 powders.

(a) New/aged powders (b) Extremely aged powders

Fig. 2. Powders coated on the powder bed.

shown in Fig. 2 (a), new powders and/or aged powders could be coated well with a smooth surface on the powder bed, which is conducive to part densification and consolidation. Nevertheless, the extremely aged powders could not be coated smoothly because of the existence of the aggregated large particles, as shown in Fig. 2 (b), as a result of striking drop in flowability. This was attributed to an increase in the molecular weight, originating from a cross-linking of the polymer material, and an increase of particles of non-spherical, irregular shapes with featured rough edges in extremely aged powders [4]. Preprocessing of extremely aged powders is therefore necessary for a smoother coated surface and improved sintering behaviors.

In this work, a sieving process was applied to the extremely aged powder prior to printing. This process was done in a fume hood using a sieve with the mesh size of 200 μm to grind the powders. The time for sieving a batch of 500 ml powders is around 2 h with preparation and post cleaning procedures. After the sieving process, about 50 ml ~ 80 ml heavy materials were captured. In all, 84 % ~ 90 % of the processed materials can be collected and reused.

2.1.3. Powder mixing

Four different groups of powders were used in experiment (as shown in Fig. 1): pure powders, mix of new and aged powders, mix of new and extremely aged powders, and mix of new, aged and extremely aged powders, to be specific. For the pure powders, 100 % new, 100 % aged, and 100 % extremely aged powders were prepared. For the mixed powder groups, powders were prepared with various mixing percentages (Fig. 5). Volume percentages are used in this paper to mix powders.

2.2. Powder characterizations

The particle size/shape distribution were measured using a PartAn 3-D particle size and shape analyzer, as shown in Fig. 3. The measurement range of the analyzer is from 22 microns to 35 mm, and it is suitable for the nylon particles, whose average diameter is around 50 ~ 60 μm [28,29]. New, aged, and extremely aged polyamide 12 powder samples were examined using the analyzer. To get reasonable test results, over 500,000 particles were measured in each experiment.

Scanning electron microscope (SEM) was carried out to evaluate the variations in micro surface morphologies of the collected powders in different degradation degrees. We used a Teneo LVSEM, and coated the samples with a thickness of 3 nm of Pt/Pd to increase material conductivity. We then examined these powders under different magnifications, to be specific, 200, 500, 2000 and 10,000.

To measure the thermal properties, including glass transition temperature, melting temperature, melting enthalpy, crystallization temperature, and crystallization enthalpy, we conducted Differential scanning calorimetry (DSC) on the powder samples of different degradation degrees using a TA Instruments DSC Q20. Heating and cooling cycles were performed between room temperature and 225 °C with a rate of 10 °C/min under a nitrogen atmosphere. The DSC results were obtained as guidance for experimental parameters when sintering aged or extremely aged powders.

To measure the differences of molecular components and the chemical microstructures between new and reclaimed materials, we applied Fourier-transform infrared spectroscopy (FTIR) to measure infrared absorption and emission spectra of the powders at different wavelengths. We used a Nicolet Magna-IR 560 FTIR instrument with the wavelength ranges from 6500 cm^{-1}-100 cm^{-1} and with the spectral resolution of 0.35 cm^{-1}, which is primarily used for polymer identifications. Wavelengths in the different infrared regions can be absorbed by materials with specific molecular components or microstructures. Thus the ranges of wavelengths absorbed are used to determine the sample molecular components or microstructures.

In this work, we use X-Ray diffraction (XRD) to check crystalline properties of different polyamide 12 materials, focusing specifically on changes in polymer crystallinity, crystalline phases, crystallographic structures, grain sizes and crystal orientations. XRD patterns were obtained on a D2 Phaser diffractometer (Bruker, German) with CuK_{α} radiation ($\lambda = 1.54060$ Å).

2.3. Parameter control

The parameters for new polyamide 12 powders failed to create parts with extremely aged powders. We tested different printing parameters to obtain optimal results for different powders. Fig. 1 shows six parameters that impact significantly part qualities and were used in this study: preheating temperature, laser power, laser speed, scan spacing, layer thickness, and layer numbers. These parameters were accurately controlled by our in-house developed SLS testbed in experiments. In our study, the same six core parameters are needed for consistent comparison. A variety of parameter settings are suitable for new powders, while few parameter settings are applicable to the cases when using extremely aged powders due to the degraded material properties. In particular, excessive laser power and energy density, along with a high preheating temperature, lead to over melting and deteriorated part properties when sintering extremely aged powders. The general principles to select the optimal parameter settings in this work are that (i) the parameters are set as close to OEM recommendations for regular printing as possible, and (ii) the new, aged and extremely aged polyamide 12 powders can all be successfully printed into parts using the same set of parameters. The selected optimal parameter settings suitable for powders of different degradation levels are: 160 °C preheating temperature; 3000 mm/s scan speed; 18 W laser power; 0.3 mm scan spacing; and 150 μm layer thickness. In our testing, we printed 10-layer tensile bar samples for each powder combination.

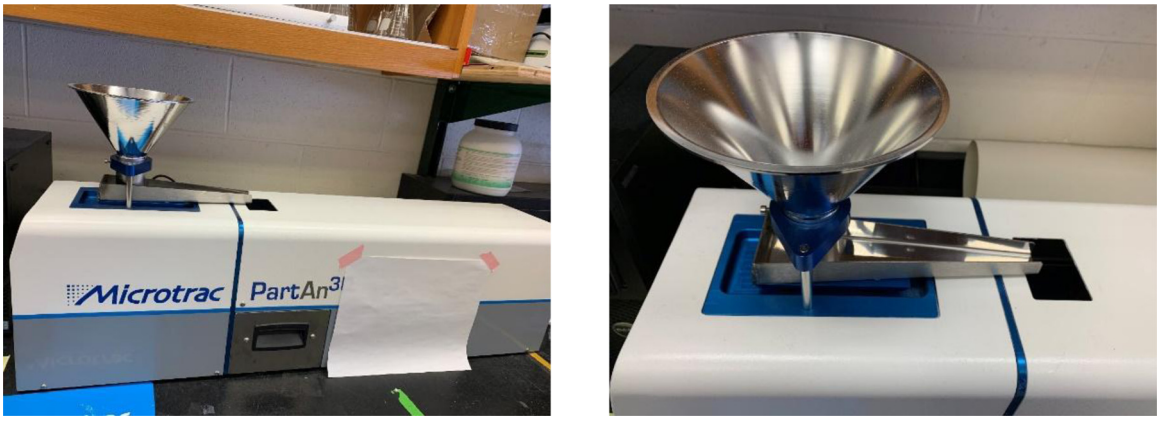

Fig. 3. A 3D particle size and shape analyzer.

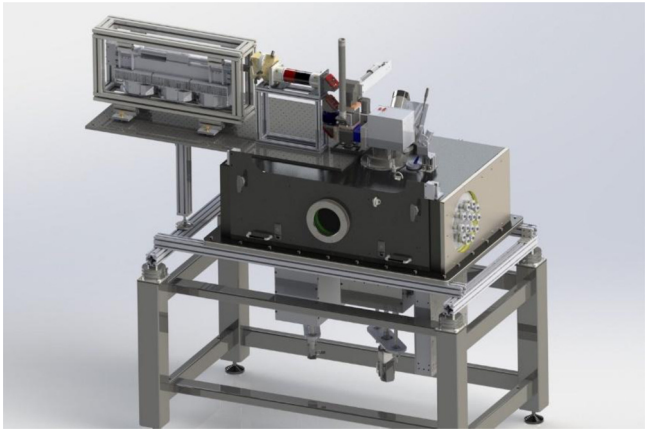

Fig. 4. In-house built and customized SLS testbeds.

2.4. SLS with interlayer heating

2.4.1. SLS machine

The SLS machine used in the paper is an in-house built open-configuration SLS AM machine/research testbed, as shown in Fig. 4. Compared to the black box commercial systems, it enables researchers to access as well as manipulate key manufacturing process parameters, build online implementable process models, and discover problems in the complex multi-physical laser sintering process. We designed the machine using a Coherent GEM100A CO_2 laser (the maximum laser power 100 W) and a Scanlab intelliSCAN 14 scanner. The powder bed dimension designed is 250 mm (L) x250 mm (W) x150 mm (H) with the layer thickness resolution of 20 μm and theoretical XY positioning resolution of 0.24 μm. The designed typical scan speed is 3.75 m/s and the maximum scan speed is 30 m/s. The powder handling is carried out by one feed cylinder, one build cylinder, and a recoating arm, which are driven by servo motor and leadscrew transmission. It is featured with combined heating method: radiation heating with infrared heaters above the powder bed (200 mm) and conduction heating with a mica heater underneath the powder bed. The software used to control the machine is an in-house developed LabVIEW program integrated with Scanlab RTC5 API, which can read G-code and send motion command to galvo scanner.

2.4.2. Proposed SLS with interlayer heating

The SLS with interlayer heating proposed in this paper is a process that interlayer heating is applied to the specimens being printed during the SLS process. Between the printing of every two layers, the proposed process maintains the surface temperature of the powder bed the same as the preheating temperature (160 °C) for a controlled period of time. We tested 0 s (no additional interlayer heating) and 60 s interlayer heating to powders and powder mixtures with different degradation levels to explore the influences of interlayer heating on part mechanical properties. Through the experiment results, it was verified that 60 s interlayer heating can provide samples with enough heat and energy.

We explored the reusability of aged and extremely aged powders and the influences of interlayer heating on part properties, as shown in Fig. 5. The experiments were separated into six stages, with a distinguish objective for each stage. In the experiment in stage 1, pure powders were used to verify the feasibility of multi-layer printing with reclaimed powders. In stage 2, the currently available industrial reuse combination, 50 % − 50 % new-aged mixed powders were used to print the benchmark samples – samples whose mechanical properties were regarded as the baselines in this research. The aim of stage 3 was to check the part mechanical properties when using new-extremely aged mixed powders with the percentages of extremely aged powders increasing. In stage 4, to examine the influences of interlayer heating on part mechanical properties, all the mixed powder combinations in stages 2 and 3 were reapplied and were printed with 60-second interlayer heating. By comparing the mechanical properties of samples in stages 2, 3, and 4, information on influences of interlayer heating on part properties were obtained. In stage 5, different from the previous stages using the combinations of *two* kinds of powders, parts were printed with mixed powders composed of all *three* types of powders to verify the feasibility and potential benefits of this practice. To ensure part quality, we selected the combinations of 30 % new - 30 % aged - 40 % extremely aged powders and 30 % new - 40 % aged - 30 % extremely aged powders. To examine the influences of interlayer heating, the experiments in stage 5 were repeated with 60-second interlayer heating in stage 6.

2.4.3. Mechanisms of SLS with interlayer heating

Due to the existence of particles with high melting points, the reclaimed polyamide 12 powders are more difficult to melt than new polyamide 12 powders. This has been verified through the hot stage microscopy and the DSC test, where the aggregated spherulite structures and high melting point pieces cannot melt during the regular sintering process [4]. Lack of coalescing polymer chains, insufficient consolidation, partial densification and numerous unmolten particles can thus appear, severely degrading the end mechanical properties. The proposed SLS with interlayer heating aims to provide the needed heating energy to promote coalescence of polymer powders and improve part densification. In the mean time, increased diversity of grain sizes in the mixed new-reclaimed powders can improve part tensile strengths when using reclaimed polyamide 12 powders.

Post-crystallization and recrystallization are different phenomena related to powder aging. Due to post-crystallization, crystallization ratio increases and spherulites grow in reclaimed powders. Recrystallization refers to the transfer of crystalline structures. Both post-crystallization and recrystallization can occur during the SLS process, although it remains unknown which one is dominant. The combined post-crystallization and recrystallization could affect part microstructures such as crystalline ratios and crystal sizes. Parts with small crystal sizes have increased flexibility and decreased brittleness, while parts with larger crystal sizes are easier to break before the separation of crystals. This study will explore the influences of interlayer heating and powder qualities on part microstructures when using reclaimed powder materials (e.g. crystalline ratios and crystal sizes, and part elongation at break).

2.5. Part characterizations

Tensile tests were carried out on all the SLS fabricated samples in Fig. 5. The samples were designed based on ASTM standards and were stretched for each tensile measurement using an Instron 5869 Electromechanical testing system with a maximum load frame capacity of 50 kN equipped with Blue Hill control software, as shown in Fig. 6. A polishing treatment was done on both the top and bottom surfaces of part to remove any skirmish un-sintered particles prior to the tensile testing for accurate measurement. We used a disc-shaped polishing machine with the diameter of 35 cm and a rubber polishing pad in the polishing treatment. The machine can rotate with running water above to clean the un-sintered particles on the surface of the tensile bars by friction. After polishing to clean the samples for proper surface measurements, tensile tests were conducted using an Instron 5869 Electromechanical testing system at a testing speed of 5 mm/min. After the tensile test, the stress-strain curves, tensile strength, elongation at break, and Young's modulus of various parts were reported.

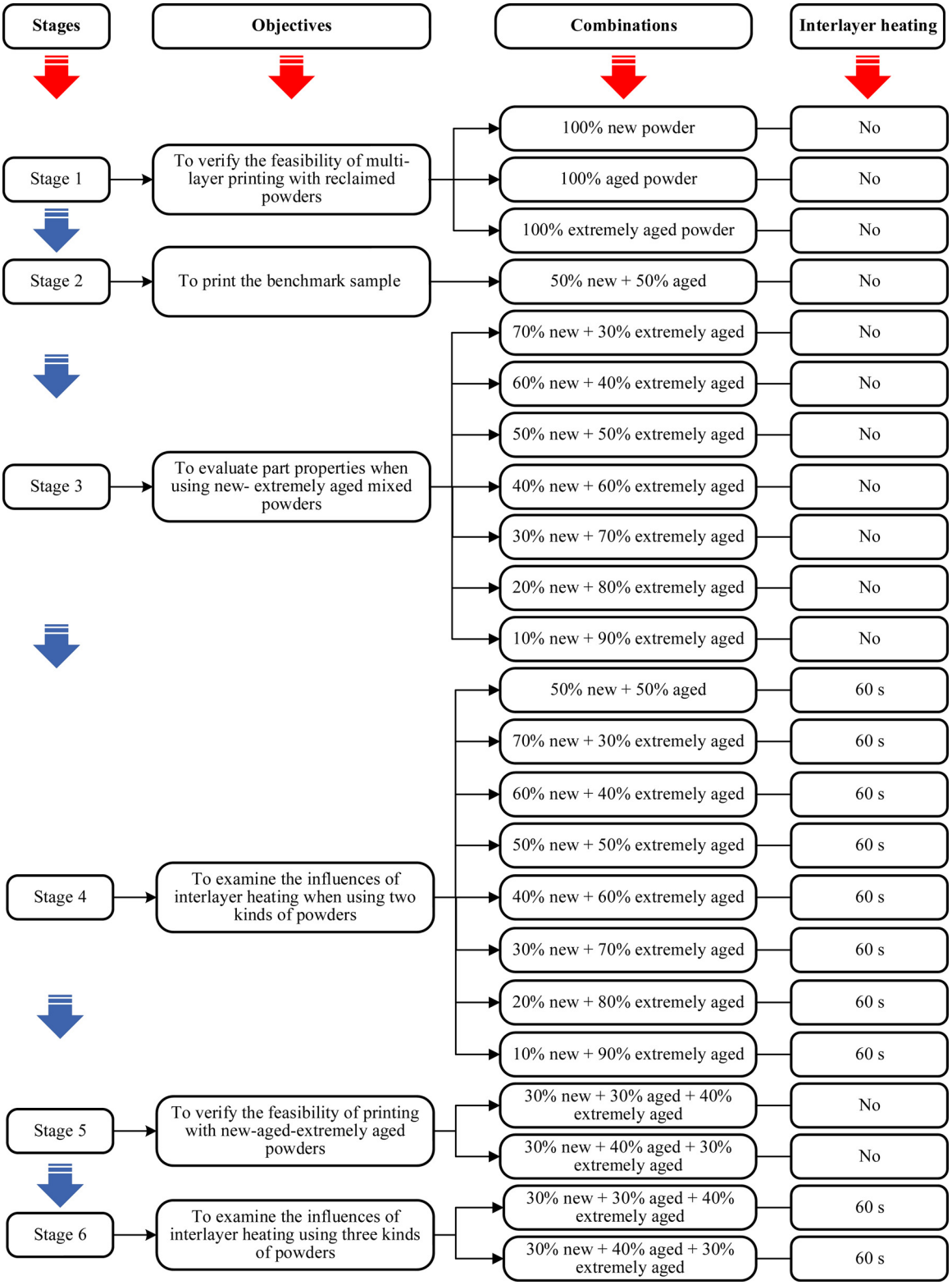

Fig. 5. Experiment plans about reusability of aged and extremely aged powders and influences of interlayer heating (The mixed powders are in volume percentages).

3. Results and discussions

3.1. Powder test results

3.1.1. Particle size/shape distribution

The particle size distributions are shown in Fig. 7. As seen, the percentages of the particles with the diameter greater than 100 μm are 21 %, 22 %, and 24 % for new powder, aged powder, and extremely aged powder, respectively, showing a mild increase after the physical/chemical degradations. The most possible explanation is that the elevated temperature and high-energy laser form an enclosed environment which leads to edge melting of the un-sintered powders, and even aggravated aggregation, leading to the increase of particle size.

The obtained particle shape distributions are shown in Fig. 8.

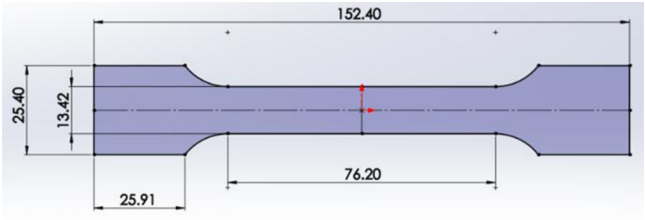

(a) Tensile bar dimensions (unit: mm)

(b) Tensile test machine - Instron 5869

Fig. 6. Tensile bar dimensions and tensile test machine.

Sphericity is the measurement of how close the shape of an object approaches that of a mathematically perfect sphere, of which the value is 1.00. In this paper, to analyze the particle shape distribution, the particles with sphericity between 0.9 ~ 1.0 are defined as particles with good sphericity. Fig. 8 shows that the percentages of particles with good sphericity for new, aged, and extremely aged powders are 21 %, 16 %, and 14 %, respectively. The sphericity of the reclaimed powder decreases mildly, which eventually increases part surface roughness. In other words, the percentage of particles with non-spherical and irregular shapes or rough edges increases, which is also a reason for the decreased flowability of the reclaimed powders.

Comparing to the new powders, a mild increase on the particle size distributions and a mild decrease on the particle sphericity distributions of the reclaimed powders are part of the reasons for the aggregated large particles and decreased flowability. In particular, a sieving process prior to printing is needed for the severely degraded extremely aged powders.

3.1.2. SEM

The SEM results of new, aged and extremely aged polyamide 12 powders are presented in Fig. 9. Each row shows the images of the same sample at different magnifications. Each column shows images of different samples at the same magnifications. In Fig. 9 (a), with the magnification of 200, little differences were observed for the three samples. In the second column, few aggregated large size particles were found in new powders, while there were more large size particles found in aged powders and extremely aged powders as aggregation exacerbated. At a magnification of 2000, more apparent differences emerged among different samples. There were no cracks in new powders, obvious cracks in aged powders, and more cracks in extremely aged powder in the SEM scope. These cracks were attributed to the evaporation of moisture or alcohol during the heating/sintering cycles or repeated expansions/shrinkages during multiple times recycling. The SEM results in Fig. 9 help us to understand the aging mechanisms of polyamide 12 powders and the effects of aging on different surface morphologies between new powders and reclaimed powders.

3.1.3. DSC

Thermal characteristics of new, aged and extremely aged polyamide 12 powders tested by DSC instrument are shown in Table 1, (a) Heating cycle and (b) Cooling cycle. Each sample went through two heating cycles and one cooling cycle. In the first heating cycle, the onset melting temperatures decrease from new powder to extremely aged powder, which is important knowledge for parameter settings of SLS printing when the aged or extremely aged powders are used. The setting principle of the preheating temperature is that the preheating temperature should be set close to the material onset melting temperature or melting point [3,20,30]. The decrease of onset melting temperature of aged and extremely aged powders gave us significant instructions when printing aged or extremely aged powder because the appropriate setting of preheating temperature is dominant to keep the sintering processes going and to ensure the part quality. A higher preheating temperature leads to unnecessary powder melting in the chamber, and a lower preheating temperature decreases the coalescence behaviors of particles. Furthermore, the decrease of the onset melting temperatures is consistent with the conclusions that aging can enlarge the melting intervals, which is caused by post-condensation. In the first heating cycle, the increase of the melting temperatures and melting enthalpies of reclaimed powders originates from the post-crystallization [16]. This is a process starting with nucleation, followed by spherulite growth. As temperature decreases, spherulites grow and radiate from the center of the core, forming spherical shapes [31] and consequently leading to the formation and aggregation of crystallites. These changes affect the melting temperatures and melting enthalpies of reclaimed powders.

3.1.4. FTIR

FTIR test results of polyamide 12 powders are presented in Fig. 10, and the infrared bands and the corresponding assignments are exhibited in Table 2. In polyamides, CH bonds close to nitrogen are the weakest bonds, thus most oxidation reactions proceed on these carbons [31,32]. In the FTIR spectra, the existence of peaks at 1368, 1158, 1062 and 946 cm^{-1}, and the corresponding dramatically diminished signals after printing reveal the oxidation reactions occurred on carbons close to nitrogen [3]. In Fig. 10, peaks at the vibrational frequencies of 1369.23, 1159.03, 1062.60 and 948.82 cm^{-1} slightly decreased in aged powders and extremely aged powders compared to new powders, which was a sign of oxidation reactions. Therefore, similar to the material aging after the sintering process, the aging mechanisms of the recycled powders impacted by the existence of laser and high temperature are thermal oxidations.

In the long molecular chains, every 12-carbon can be regarded as a polyamide 12 unit with only one carbon and oxygen double bond, forming the basic molecular structure of the new polyamide 12 powders. In each polyamide 12 unit, C—H bonds in the methylene groups adjacent to the nitrogen are the weakest bonds. Free hydrogen molecule radicals can emerge from these carbons in the presence of laser radiations to initiate the oxidation process. During the propagation process of oxidation reactions, unavoidable oxygen residual in the chamber (2 %–5 % in state of the art [4]) gets absorbed, forming unstable middle products or structures such as peroxide radicals and peroxides. After the termination of the oxidation reaction with stable final products, two carbon and oxygen double bonds exist in every polyamide 12 unit due to the addition of oxygen in reclaimed powder in contract to the new

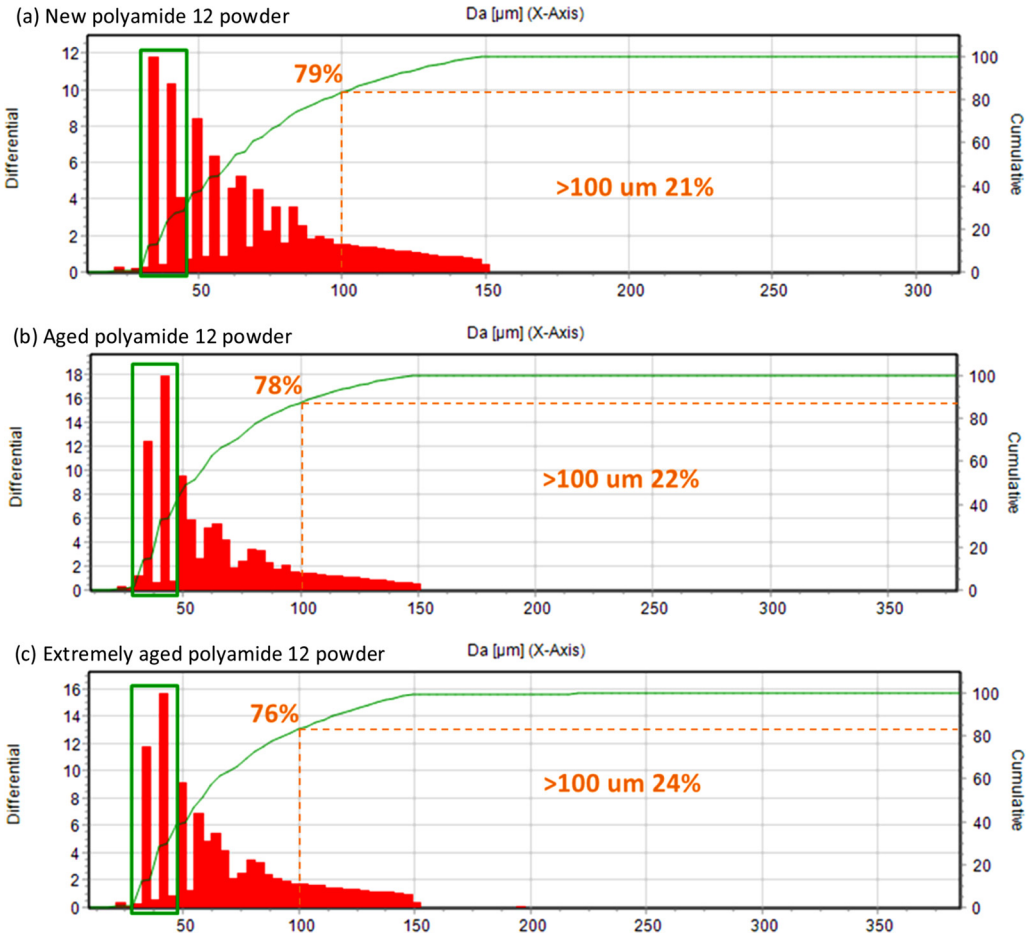

Fig. 7. Particle size distribution of polyamide 12 powders.

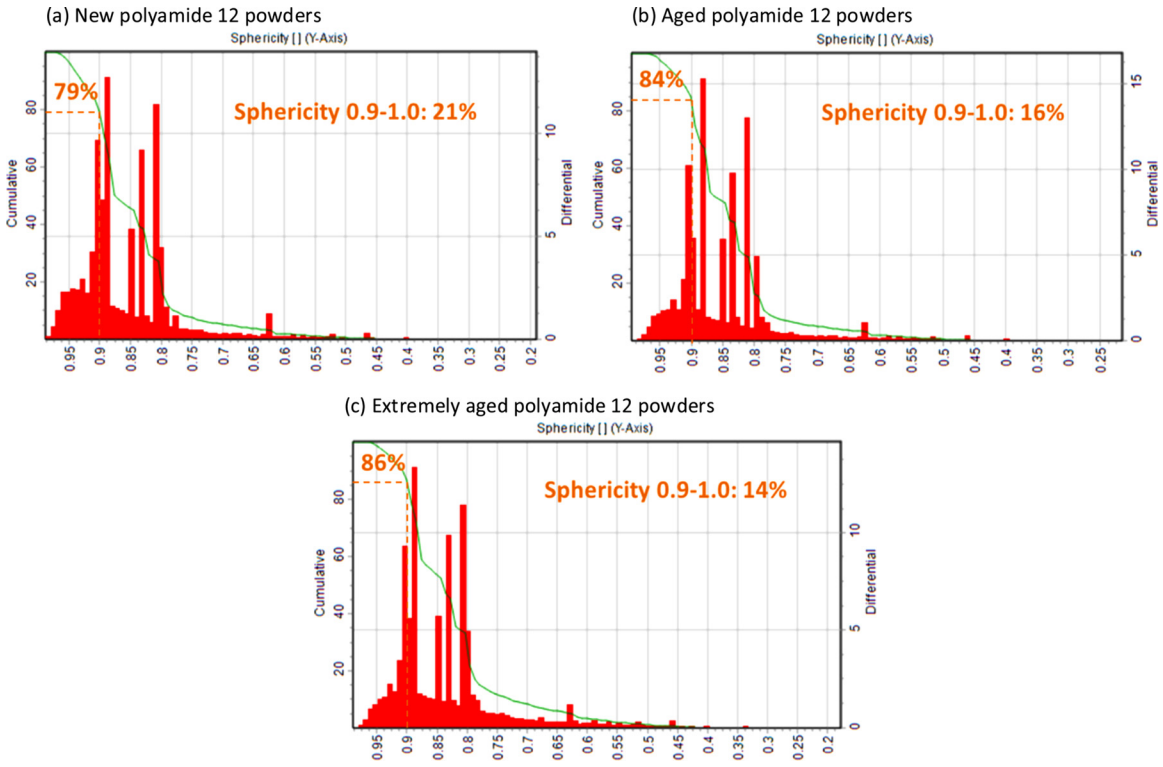

Fig. 8. Particle shape distribution of polyamide 12 powders.

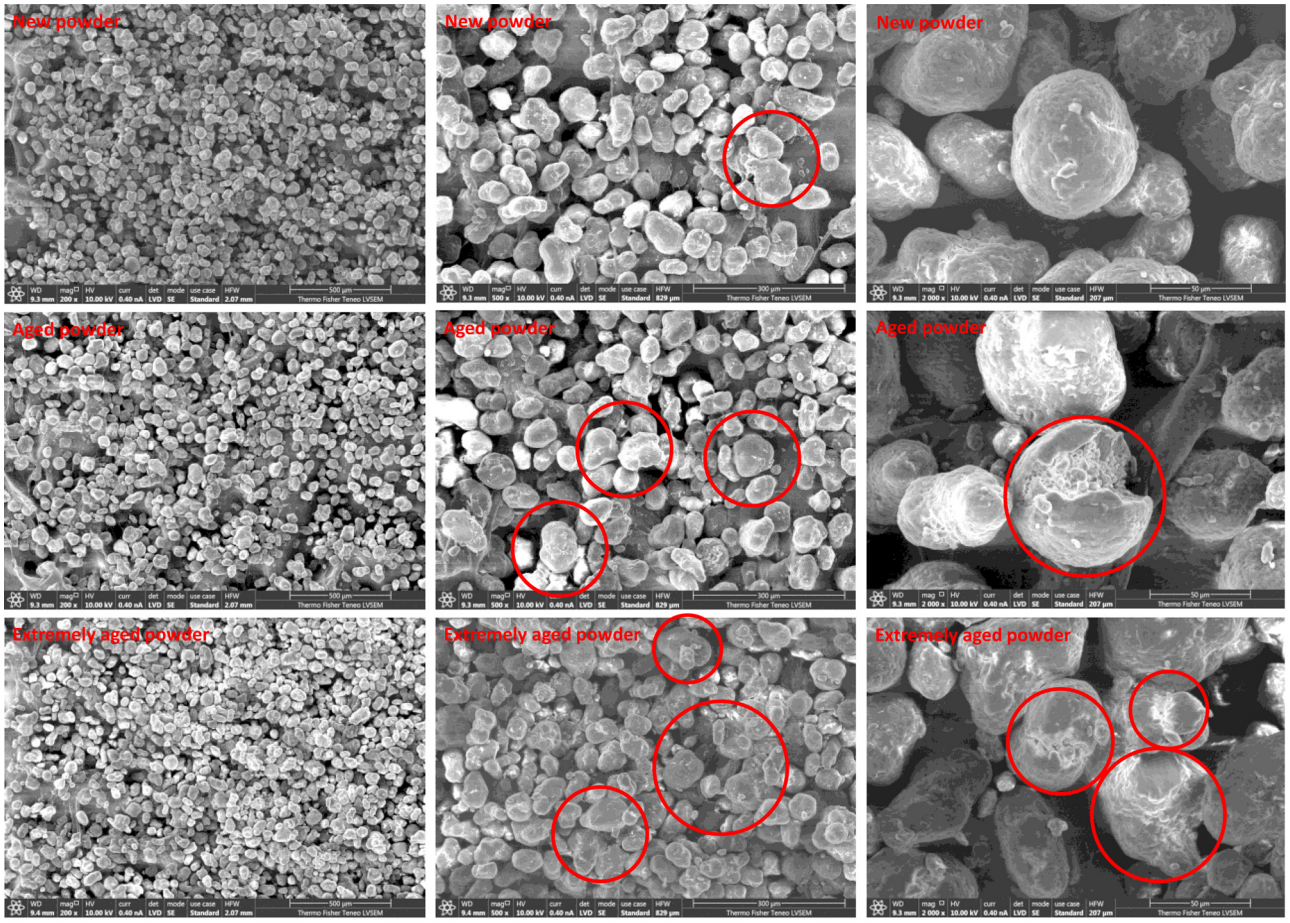

(a) 200 magnification (b) 500 magnification (c) 2000 magnification

Fig. 9. SEM results of polyamide 12 powders.

Table 1
Thermal characteristics of new, aged and extremely aged polyamide 12 powders.

(a) Heating cycle

Polyamide 12 powder	Heating process	Onset melting temperature/°C	Peak melting temperature/°C	Melting enthalpy/J·g^{-1}
New powder	The first heating cycle	183.36	186.38	97.60
	The second heating cycle	172.48	177.55	41.25
Aged powder	The first heating cycle	181.81	188.18	104.7
	The second heating cycle	171.38	176.97	41.42
Extremely aged powder	The first heating cycle	180.77	187.71	103.3
	The second heating cycle	170.82	176.62	35.69

(b) Cooling cycle

Polyamide 12 powder	Cooling process	Onset crystallization temperature/°C	Peak crystallization temperature/°C	Crystallization enthalpy/J·g^{-1}
New powder	Cooling cycle	152.14	148.23	50.15
Aged powder		150.40	146.48	48.42
Extremely aged powder		150.97	147.02	46.78

powders [3].

Due to the oxidation reaction, the molecular structures of reclaimed polyamide 12 powders are more complex and stable. It is consistent with the conclusion from the DSC test that the melting temperatures and melting enthalpies of reclaimed powders increase. After the oxidation reaction, or the addition of oxygen to the molecular chains of polyamide 12 powders, the molecular weight of the materials may increase. It has been verified that long build time and high build temperature leads to a molecular weight increase of reclaimed polyamide 12 powders [22].

3.1.5. XRD

XRD test results of polyamide 12 powders are shown in Fig. 11, indicating crystalline structures of the new and deteriorated polyamide 12 powders. Polyamide 12 exhibits two crystal structures, α and γ phases, and usually γ acts as its stable phase. As shown in Fig. 11, the XRD test results of new, aged, and extremely aged polyamide 12 powders presented similar behaviors and are in different colors. The XRD peak at 10.98° was selected as a reference of crystallization. These curves all exhibited α-structures with very high crystallinities, unstable structures and oriented in an anti-parallel manner, which were

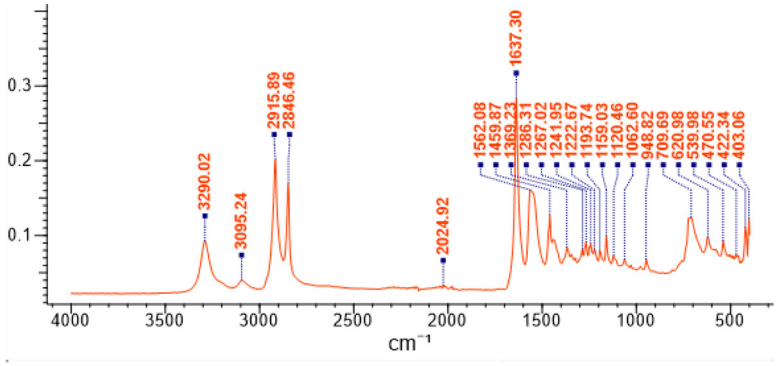

(a) New polyamide 12 powder

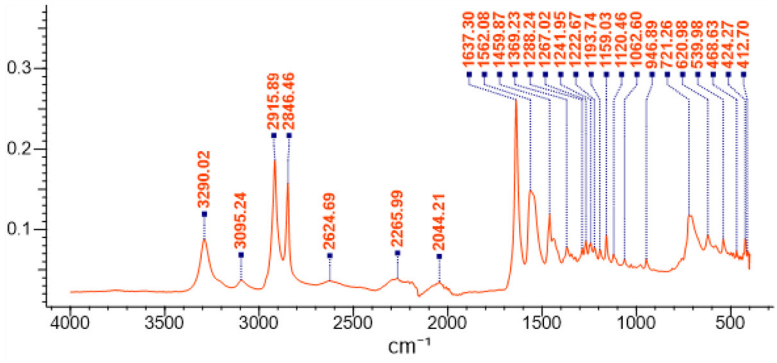

(b) Aged polyamide 12 powder

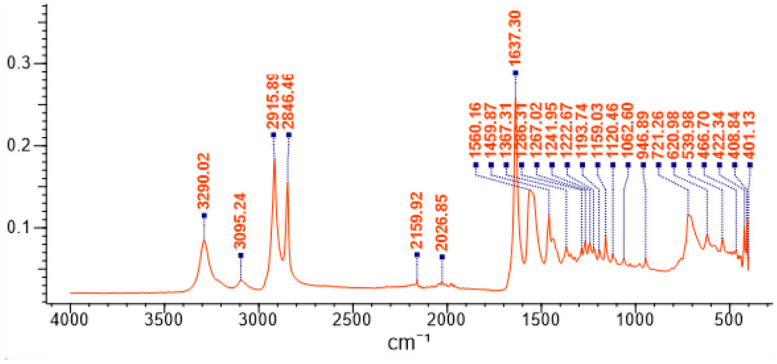

(c) Extremely aged polyamide 12 powder

Fig. 10. FTIR results of polyamide 12 powders.

Table 2
Infrared bands and the assignments.

Vibrational frequency (cm^{-1})	Assignments
3290.02	−NH stretching vibration
3095.24	Fermi resonance of the ν(NH−) stretching
2915.89	CH_2 asymmetric stretching
2846.46	CH_2 symmetric stretching (ordered)
1637.30	Amide-I (mostly of the ν(CO═) stretches)
1459.87	CH_2 reference band
1369.23	CH bend, CH_2 twisting
1267.02	Amide III (C-N stretching + C═O in-plane bending)
1193.74	Splitting of amide II (CH_2 wagging or CH_2 twisting)
1159.03	Skeletal motion involving CONH (am, γ)
1062.60	Skeletal motion involving CONH
948.82	CONH in-plane
709.69	CH_2 rocking
620.98	Amide VI (N−H out-of-plane bend)

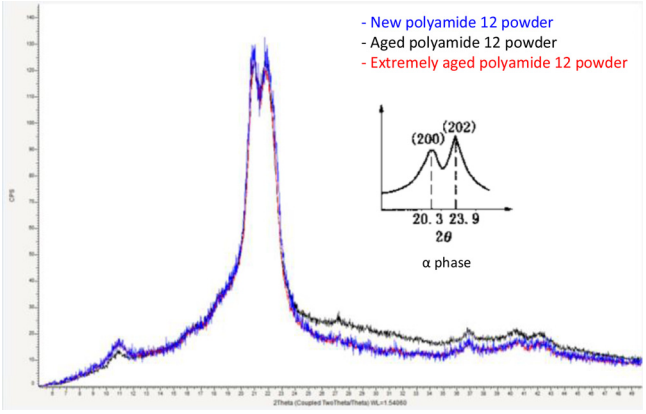

Fig. 11. XRD test results of polyamide 12 powders.

Table 3
Printing results about reusability of extremely aged powders and influences of interlayer heating.

Stages	Powder percentages	Interlayer heating	Sample number	Thickness / mm
Stage 1	100 % new powder	No	3	0.88; 0.82; 0.81
	100 % aged powder	No	2	0.91; 0.91
	100 % extremely aged	No	2	0.65; 0.68
Stage 2	50 % new + 50 % aged	No	3	1.41; 1.41; 1.40
Stage 3	70 % new + 30 % extremely aged	No	2	1.46; 1.45
	60 % new + 40 % extremely aged	No	2	1.25; 1.25
	50 % new + 50 % extremely aged	No	3	0.98; 0.97; 0.96
	40 % new + 60 % extremely aged	No	3	1.43; 1.42; 1.41
	30 % new + 70 % extremely aged	No	2	1.38; 1.36
	20 % new + 80 % extremely aged	No	2	1.36; 1.34
	10 % new + 90 % extremely aged	No	3	0.80; 0.78; 0.78
Stage 4	50 % new + 50 % aged	60 s	3	1.41; 1.41; 1.42
	70 % new + 30 % extremely aged	60 s	2	1.48; 1.47
	60 % new + 40 % extremely aged	60 s	3	0.82; 0.83; 1.12
	50 % new + 50 % extremely aged	60 s	3	1.42; 1.40; 1.40
	40 % new + 60 % extremely aged	60 s	2	1.36; 1.36
	30 % new + 70 % extremely aged	60 s	3	1.32; 1.35; 1.30
	20 % new + 80 % extremely aged	60 s	2	1.00; 1.00
	10 % new + 90 % extremely aged	60 s	3	1.22; 1.26; 1.14
Stage 5	30 % new + 30 % aged + 40 % extremely aged	No	3	1.40; 1.38; 1.40
	30 % new + 40 % aged + 30 % extremely aged	No	2	1.34; 1.35
Stage 6	30 % new + 30 % aged + 40 % extremely aged	60 s	3	1.40; 1.39; 1.36
	30 % new + 40 % aged + 30 % extremely aged	60 s	2	1.26; 1.33

*Preheating temperature, 160 °C; scan speed, 3000 mm/s; laser power, 18 W; scan spacing, 0.3 mm; layer thickness, 150 μm.

consistent with reference results [3,4].

3.2. Printing results

Based on the proposed method, the tensile bars with 10 layers were printed. Using differently degraded materials, the same series of optimized parameters were applied to all the designed experiments in Fig. 5 to ensure the equivalent processing conditions. The printing results are presented in Table 3.

Though we used the same set of parameter settings to print the tensile bar samples, we recoated different combinations of powders to print different samples. Thus, there are sample variations in, e.g., coalescence behaviors, solidification and consolidation effects, yielding variable thicknesses in the generated tensile bars. Such variations, however, do not affect the measured normalized mechanical properties. The width of tensile bars is in good consistence with the dimensions designed in Fig. 6a. Note that a few samples (e.g. Fig. 12f) contain deformation in pictures. The reason is that we air cooled all samples outside the chamber after printing, instead of waiting for them to cooldown inside the chamber.

Pictures of tensile bar samples are shown in Fig. 12. The samples printed using 50 %−50 % new-aged mixed powders are taken as the benchmark parts. Samples printed using powders of different mixing ratios are listed, with and without interlayer heating. As seen, all samples were successfully 3D printed with no visible differences on the sample surfaces. More part characterizations will be explained in the following sections.

3.3. Part test results

3.3.1. Stage 1

The stress-strain curves of samples printed using pure powders are exhibited in Fig. 13. As shown, there are several differences between these samples. The average tensile strength of samples printed using new powders, aged powders and extremely aged powders are respectively 22.96 Mpa, 18.12 Mpa, and 11.08 Mpa, and that of samples using aged and extremely aged decreased by 21.09 % and 51.75 % compared to new ones. As explained in Section 2.4.3, parts using more new powders have larger tensile strength under standard settings. The average Young's modulus of samples printed using new powders, aged powders, and extremely aged powders are respectively 503.67 Mpa, 358.50 Mpa, and 177.00 Mpa, and that of samples using aged and extremely aged decreased by 28.82 % and 64.86 % compared to new ones. However, the average elongations at break of samples using new, aged, and extremely aged powders are respectively 5.31 %, 12.12 %, and 9.56 %, and that of samples using aged/extremely aged powders increase by 56.20 % and 44.46 % compared to new SLS parts. The reason for this is attributed to that the reclaimed materials have smaller crystal size, increased flexibility and decreased brittleness. Inversely, parts using new powders with larger crystal size are easier to break down before the separation of crystals, with decreased flexibility. Using the Scherrer's equation and XRD test results, we calculated the crystal sizes of the printed parts in Fig. 13. The crystal sizes of new parts, parts using aged powders and parts using extremely aged powders are respectively 5.21 nm, 3.39 nm and 4.53 nm, which are consistent with our previous conclusions.

3.3.2. Stage 2

As the most popular used mixing percentages for recycling aged powders [4], the samples printed using the 50 %−50 % new-aged mixed powders are taken as the benchmark samples in this paper, of which the mechanical properties are baselines in the proposed method. The stress-strain curves of the benchmark samples are shown in Fig. 14. There are two breakpoints in the stress-strain curves for these samples due to the layered fabrication process. For sample 1, there is a breakpoint at the strain of 7.82 %, and another at 11.57 %, indicating that layered fracture occurred during the tensile tests. This is a phenomenon that multiple layers in one tensile bar break down at different times. We recoated different combinations of mixed powders to print different samples. The mixed powders affect sample solidification and consolidation between layers and results in the layered fracture in the parts using mixed powders. Calculating the average mechanical properties of the benchmark samples, the baselines of tensile strength, Young's modulus and elongation at break are respectively 25.80 Mpa, 568 Mpa, and 11.36 %. The average mechanical properties of these samples will be used to evaluate the mechanical properties of the tensile bars in the following Stages.

3.3.3. Stage 3

In stage 3, samples using new-extremely aged mixed powders

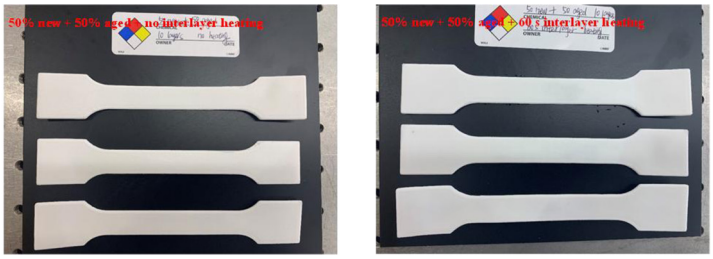

(a) Benchmark tensile bars with and without interlayer heating

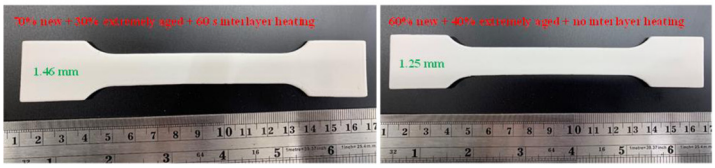

(b) Tensile bars with 30% and 40% extremely aged powders

(c) Tensile bars with 50% and 60% extremely aged powders

(d) Tensile bars with 70% extremely aged powders

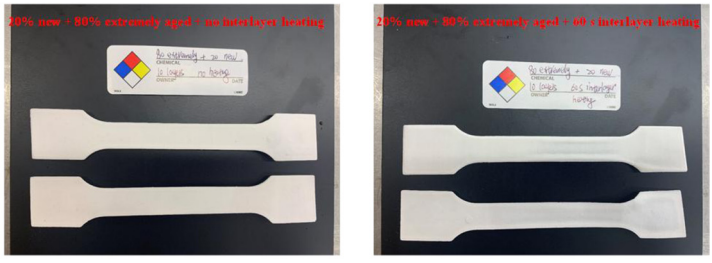

(e) Tensile bars with 80% extremely aged powders

(f) Tensile bars with 90% extremely aged powders

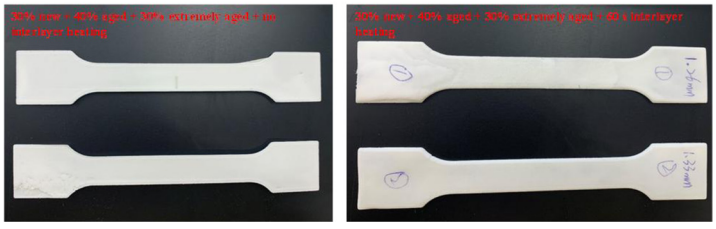

Fig. 12. Pictures of some tensile bar samples.

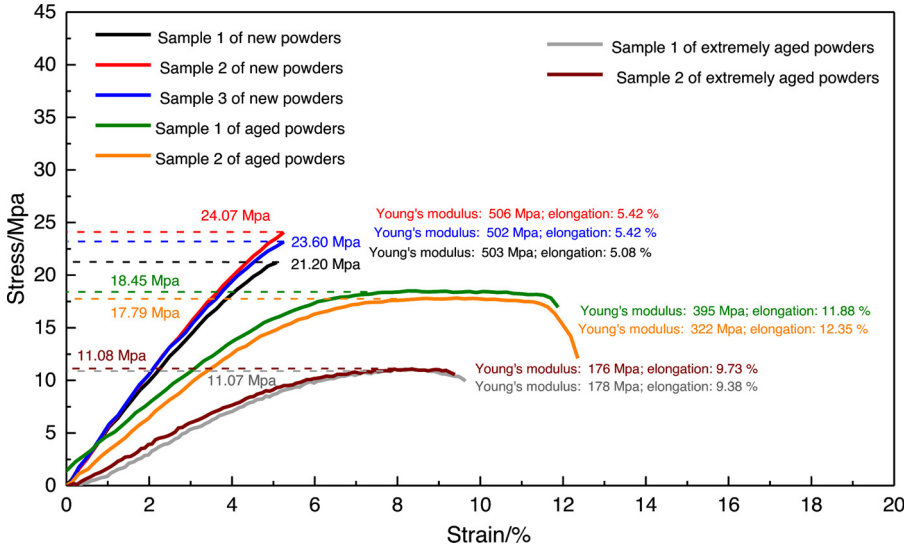

Fig. 13. Stress-strain curves of samples printed using pure powders.

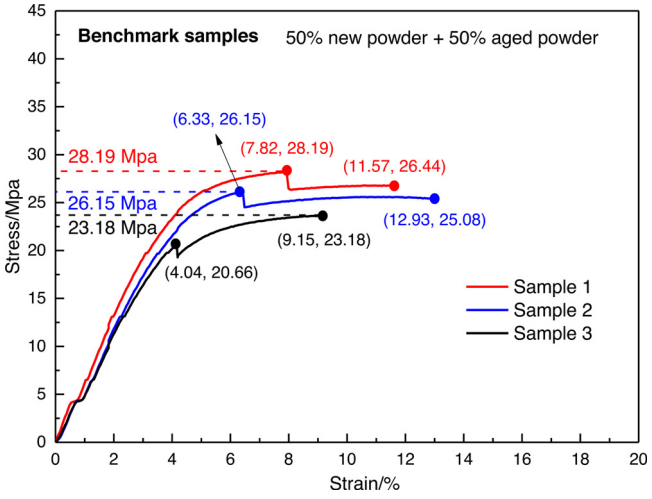

Fig. 14. Stress-strain curves of benchmark samples.

without interlayer heating were printed, and the stress-strain curves of these samples are shown in Fig. 15 (a) - (g). With the percentages of extremely aged powders increasing from 30 % to 90 %, the average tensile strengths are 24.69 Mpa, 29.18 Mpa, 25.32 Mpa, 25.02 Mpa, 20.93 Mpa, 22.65 Mpa and 29.97 Mpa, and the average elongations at break are 7.10 %, 7.76 %, 8.60 %, 8.43 %, 12.33 %, 13.38 % and 15.36 %. The average tensile strength of parts from the combination of 60 % – 40 % new-extremely aged mixed powders to the combination of 30 %–70 % new-extremely aged mixed powders show a decrease. But this did not apply to the remaining mixing percentages, which can be ascribed to that the mechanical properties of samples are not only related to the properties of powders but also relevant to the thermal or laser conditions in the sintering chamber. It is worth noting that the tensile strengths of 10 %–90 % new-extremely aged samples appear to be better than the benchmark samples. Due to the severely decreased flowability of the extremely aged powders, the recoating of the extremely aged powders is difficult. The large percentage of the extremely aged powders in the 10 %–90 % new-extremely aged mixed powders accompanied with sustained high temperature in the SLS chamber failed the recoating process during the printing of the last few layers. And the obtained top layers were sintered multiple times with no powders recoated, which has the similar effects with printing using improved energy densities. High energy densities lead to high mechanical properties. This is the reason for the large tensile strengths of 10 %–90 % new-extremely aged samples. Overall, when the percentages of new powders decrease (from 60 % to 20 %) and the percentages of extremely aged powders increase (from 40 % to 80 %), the average tensile strengths of samples decrease. However, the elongations at break increase with the increasing of extremely aged powders because the microstructure changes.

3.3.4. Stage 4

Fig. 16 compares stress-strain curves of benchmark samples and samples using new-extremely aged mixed powders with and without interlayer heating. As shown, the tensile strengths of some samples remain no significant changes after interlayer heating, while that of the other samples increase. In Fig. 16 (a)–(c), (e), (f), the tensile strengths of samples with 60-second interlayer heating increased by 25.19 %, 36.10 %, 30.13 %, 5.46 % and 22.51 %. With 60-second interlayer heating, the average tensile strengths of tensile bars printed using 50 % – 50 % new-aged powder mix, 70 % – 30 % new-extremely aged powder mix, 60 % – 40 % new-extremely aged powder mix, 40 %–60 % new-extremely aged powder mix and 30 %–70 % new-extremely aged powder mix are respectively 32.30 Mpa, 33.61 Mpa, 37.97 Mpa, 26.39 Mpa and 25.64 Mpa. With interlayer heating, tensile bars 3D printed using more new powders tend to have larger tensile strengths. In total, the tensile strengths of samples using mixed powders can be improved to some extent after interlayer heating because of the better melting and coalescence behaviors of particles on each layer. In particular, in addition to the successful reusing of extremely aged powders, the proposed process control yields parts with tensile strength 25.19 % higher than default machine configuration using the standard material combination (Fig. 16a).

3.3.5. Stage 5 and Stage 6

Fig. 17 compares stress-strain curves of samples using new-aged-extremely aged mixed powders with and without interlayer heating. After 60 s interlayer heating, the tensile strengths of samples using 30 %-30 %–40 % new-aged-extremely aged mixed powders increase by 1.19 %, and that of samples using 30 %–40 %-30 % new-aged-extremely aged mixed powders increase by 18.04 %. It is concluded that the tensile strengths of samples using new-aged-extremely aged mixed powders can be improved after interlayer heating.

3.3.6. Discussions

3.3.6.1. Tensile strength. Fig. 18 compares tensile strengths of the

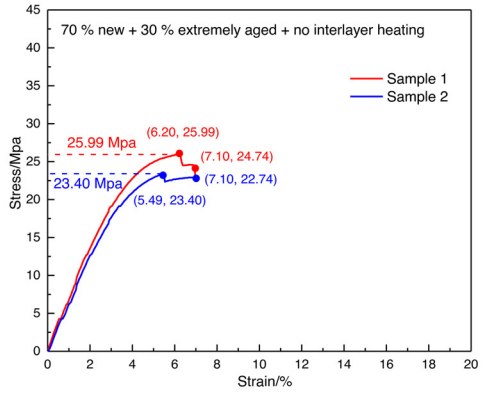

(a) 70% new + 30% extremely aged

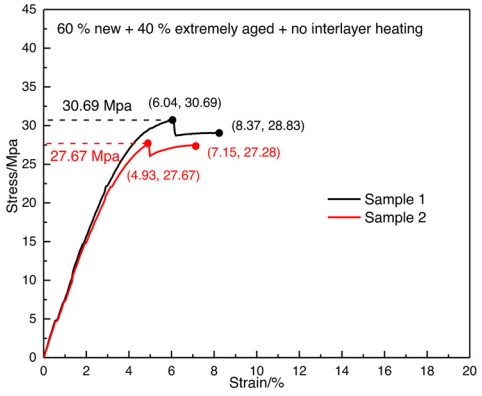

(b) 60% new + 40% extremely aged

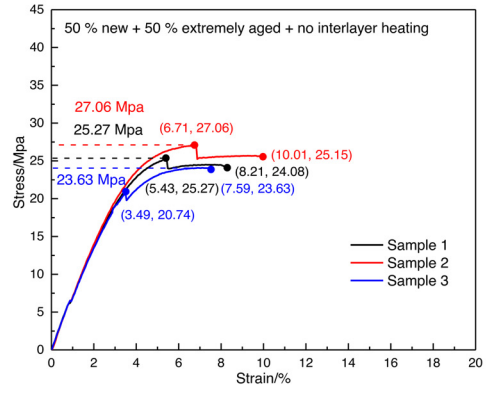

(c) 50% new + 50% extremely aged

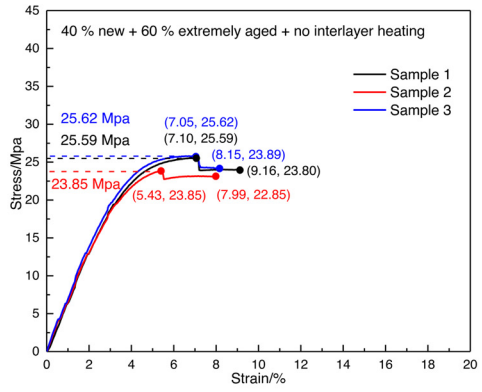

(d) 40% new + 60% extremely aged

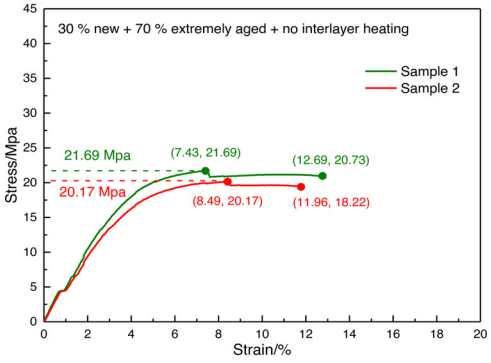

(e) 30% new + 70% extremely aged

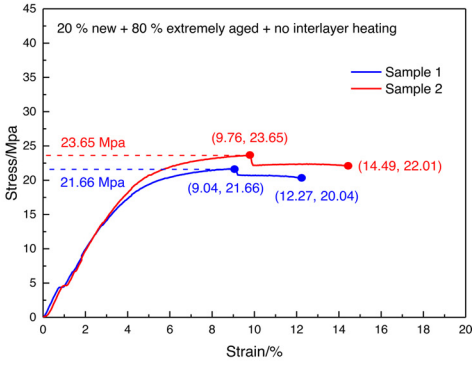

(f) 20% new + 80% extremely aged

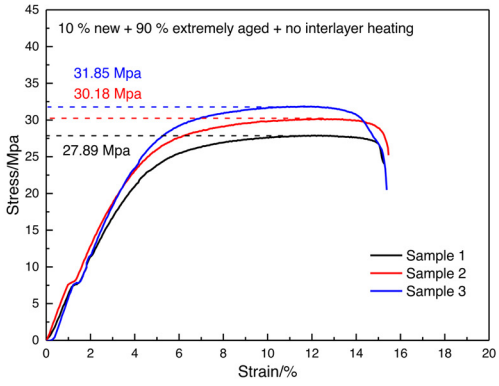

(g) 10% new + 90% extremely aged

Fig. 15. Stress-strain curves of samples printed using new-extremely aged mixed powders without interlayer heating.

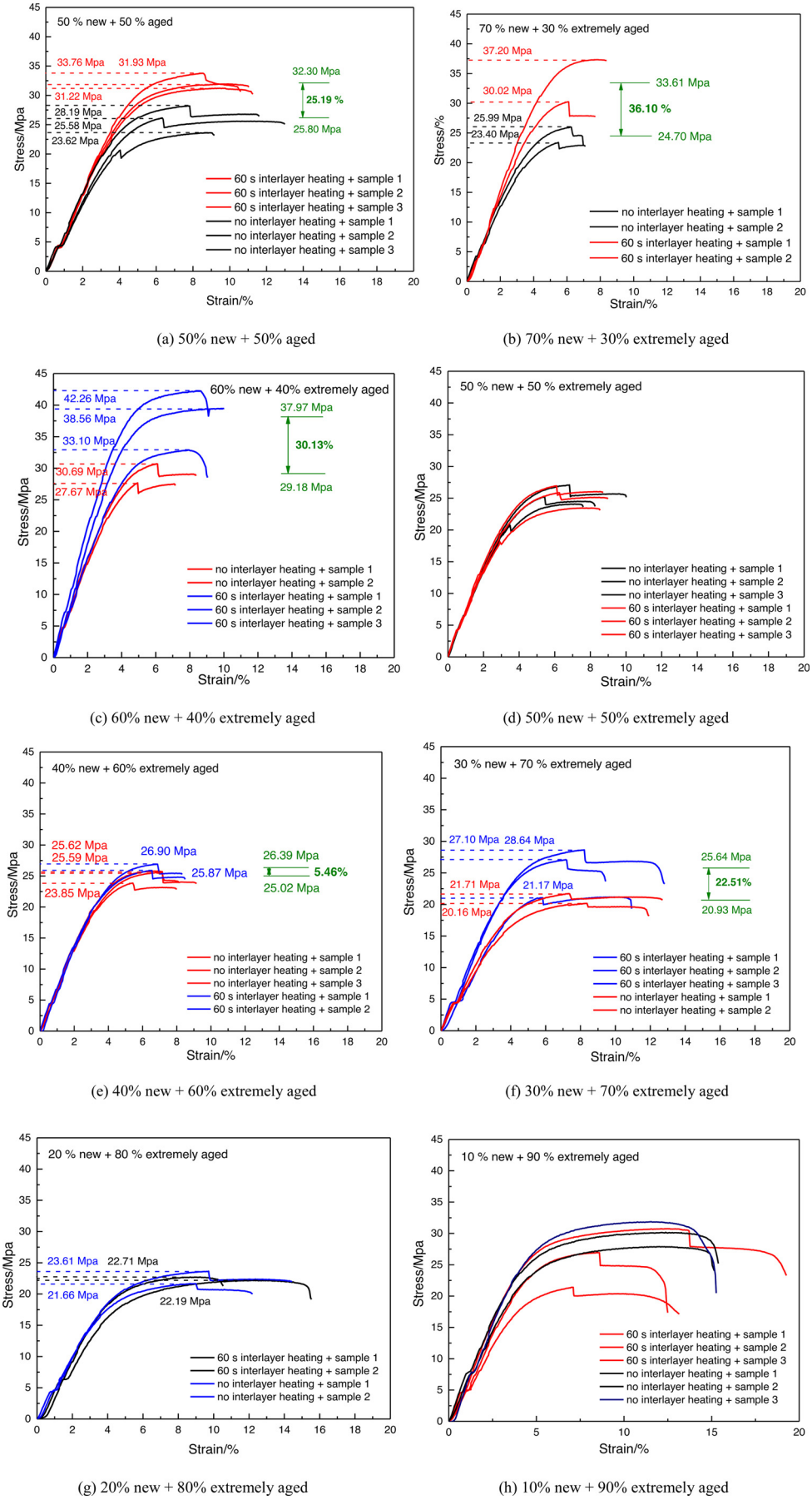

(a) 50% new + 50% aged

(b) 70% new + 30% extremely aged

(c) 60% new + 40% extremely aged

(d) 50% new + 50% extremely aged

(e) 40% new + 60% extremely aged

(f) 30% new + 70% extremely aged

(g) 20% new + 80% extremely aged

(h) 10% new + 90% extremely aged

Fig. 16. Comparisons of stress-strain curves of benchmark samples and samples using new-extremely aged mixed powders with and without interlayer heating.

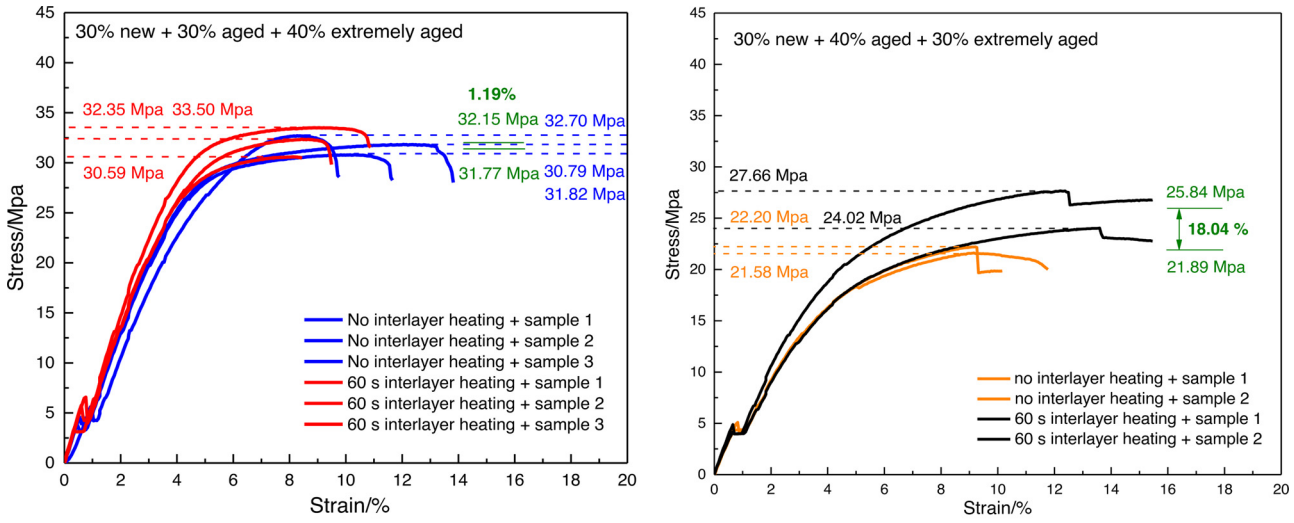

(a) 30% new + 30% aged + 40% extremely aged (b) 30% new + 40% aged + 30% extremely aged

Fig. 17. Comparisons of stress-strain curves of benchmark samples and samples using new-aged-extremely aged mixed powders with and without interlayer heating.

samples: (a) without interlayer heating, (b) with 60 s interlayer heating. The baseline here is the samples printed from the 50 %－50 % new-aged blend without interlayer heating, i.e., 25.80 Mpa. From Fig. 18 (a), the powder blends yielding larger tensile strengths than the baseline are: 40 %–60 % new-extremely aged, 30 %-30 %–40 % new-aged-extremely aged, and 10 %–90 % new-extremely aged. However, when the percentages of extremely aged powders increased from 50 % to 80 %, the average tensile strengths decrease. The reasons are that it is more difficult to move dislocations through and between the grains when there are more extremely aged powders. Therefore, *for the samples without interlayer heating, the recommended mixing percentages closest to industry current practice is* 60 %－40 % *new-extremely aged and* 30 %-*30 %–40 % new-aged-extremely aged (13.*18 % *and 23.*14 % *better than baseline)*.

From Fig. 18 (b), there are three blends with 60 s interlayer heating of which the tensile strengths are larger than the baseline (25.80 Mpa): 50 %－50 % new-aged, 60 %－40 % new-extremely aged and 30 %-30 %–40 % new-aged-extremely aged (25.19 %, 47.17 % and 24.69 % better than baseline). Thus, *the recommended mixing percentages closest to industry current practice for the samples with interlayer heating are* 50 %－50 % *new-aged,* 60 %－40 % *new-extremely aged and* 30 %-*30 %–40 % new-aged-extremely aged.*

Tensile bars using reclaimed powders cannot coalesce well due to the high melting point particles. As a result of the insufficient consolidation, partial densification and numerous unmolten particles, tensile strengths of the 3D printed parts degrade. Thus, tensile bars using more new powders normally have larger tensile strengths. In Fig. 18b, the tensile bars using 60 %－40 % new-extremely aged mixed powders with interlayer heating have more new powders and better coalescence behaviors than most of the other parts, resulting in superior tensile strength. For the tensile bars using 70 %－30 % new-extremely aged mixed powders with interlayer heating, the tensile strength is slightly lower than that of the parts using 60 %－40 % powder blend. The reason is that the tensile bars using 60 %－40 % new-extremely aged mixed powders have better densification than that using 70 %－30 % new-extremely aged mixed powders, which has been verified from our SEM test results.

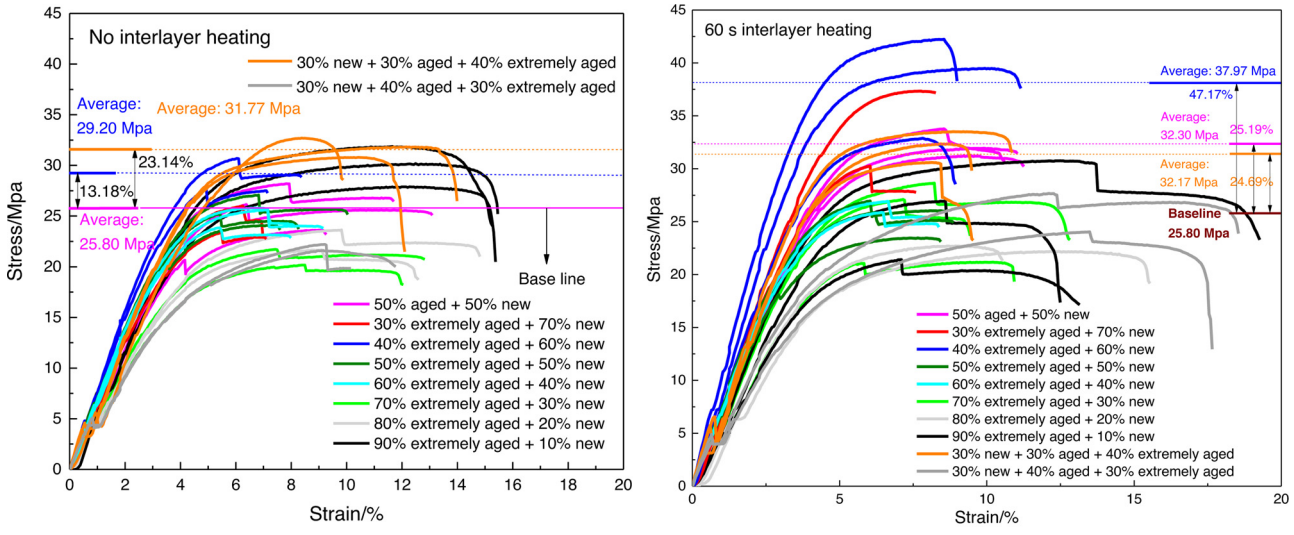

(a) Samples without interlayer heating (b) Samples with 60 s interlayer heating

Fig. 18. Comparisons of sample tensile strengths.

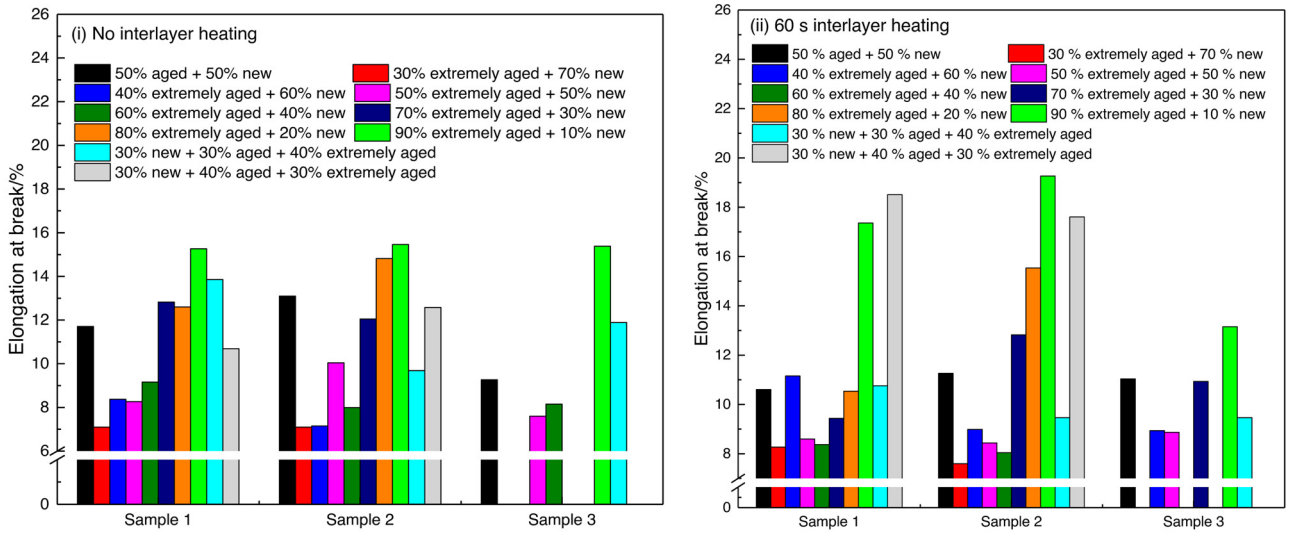

(a) Sample elongations at break

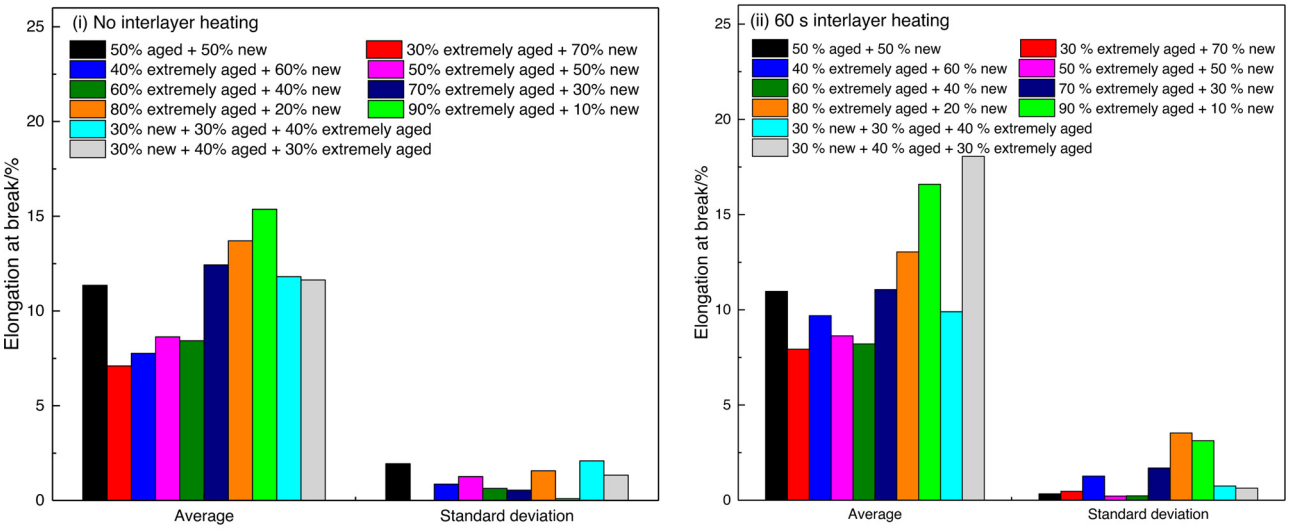

(b) Mean values and standard deviations of sample elongations at break

Fig. 19. Comparisons of sample elongations at break.

3.3.6.2. Elongation at break. Fig. 19 compares sample elongations at break: (a) sample elongations at break, (b) mean values and standard deviations of sample elongations at break. Similar to the tensile strength test, the baseline performance is from the samples printed using 50 %−50 % new-aged blend without interlayer heating, i.e., 11.36 %. From Fig. 19b, there are several blends that have similar or larger values of elongations at break compared to the baseline. For the samples without interlayer heating (Fig. 19b (i)), the samples using more extremely aged powders have larger average elongations. The largest elongation is from the 10 %–90 % new-extremely aged blend (the average value is 35.30 % better than baseline), because increased extremely aged powders yields smaller crystal size (verified by XRD) and increased flexibility. *The recommended mixing percentages of samples without interlayer heating are* 30 %-*30 %–40 % new-aged-extremely aged and 30 %–40 %*-30 % *new-aged-extremely aged mixed blends.* These combinations are close to industry current practice, and the elongations are better than baselines. For the samples with interlayer heating (Fig. 19b (ii)), the largest elongation is from the 30 %–40 %-30 % new-aged-extremely aged mixed blend (the average value is 58.97 % better than baseline), because interlayer heating enhances particle bonding and microstructures. *The recommended mixing percentage of samples with interlayer heating is 30 %–40 %*-30 % *new-aged-extremely aged mixed blend.* The part elongation at break of this combination increases by 55.29 % after interlayer heating (from 11.63 % to 18.06 %).

From Fig. 19b, the samples without interlayer heating have relatively uniform standard deviations on elongations at break. However, the standard deviations on elongations of samples with interlayer heating are irregular. These samples with 70 %, 80 % and 90 % extremely aged powders have larger standard deviations than the remaining ones.

In general, parts using more reclaimed powders have increased elongations at break, while parts using more new powders with larger crystal sizes are easier to break before the separation of crystals. Notice that 10 %–90 % new-extremely aged powder blends generated competing results regarding elongation at break. The result is attributed to the fact that the reclaimed powders have smaller crystal size, increased flexibility and decreased brittleness. However, considering combined mechanical strength and the large deviation from industrial practice,

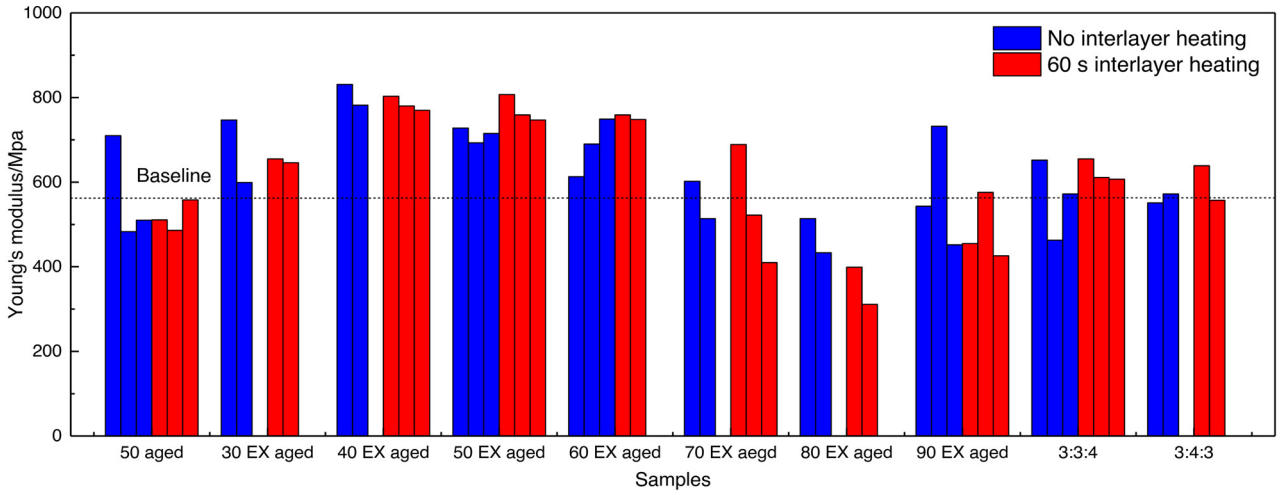

(a) Sample Young's modulus

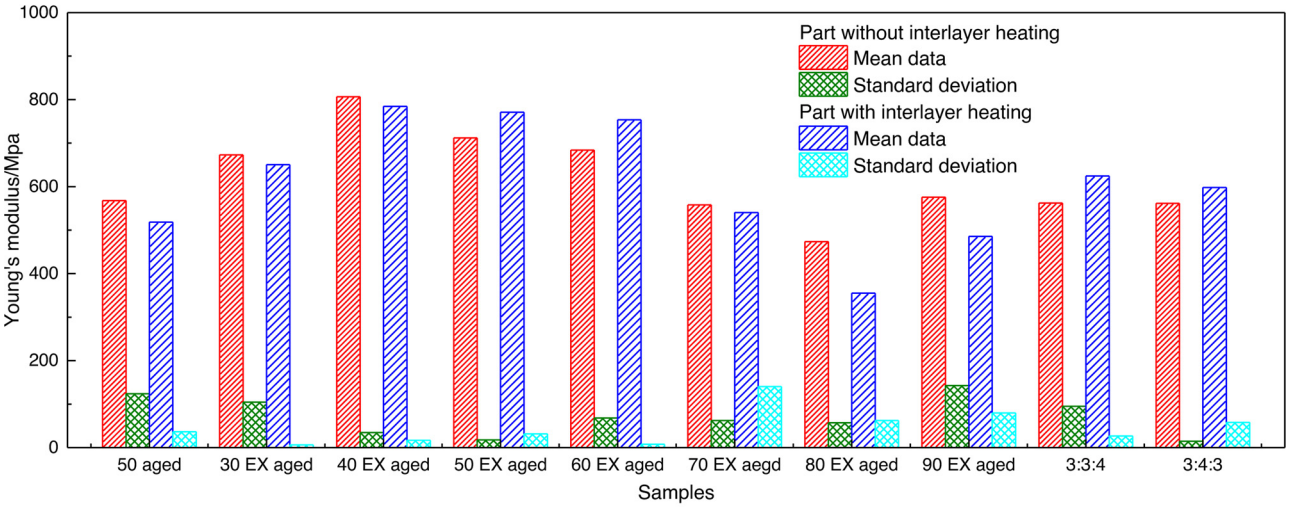

(b) Mean values and standard deviations of sample Young's modulus

Fig. 20. Comparisons of sample Young's modulus.

this powder composition is not recommended for immediate industrial application. Though parts using more reclaimed powders have smaller crystal size, increased flexibility and elongations at break, powder mixing increase diversity of grain sizes in the mixed new-reclaimed powders, contributing to decreased elongations at break.

3.3.6.3. Young's modulus and build time. Fig. 20 compares the Young's modulus of samples printed using powders of different combinations, (a) sample Young's modulus, (b) mean values and standard deviations of sample Young's modulus. The dotted line in Fig. 20a shows the Young's modulus of the 50 % − 50 % new-aged mixed blend. From Fig. 20b, parts with high percentages of extremely aged powders, for instance, 70 %, 80 % and 90 %, have lower average Young's modulus. However, there is no distinct rule that the standard deviations of sample Young's modulus are affected by powder combinations or interlayer heating. Also, in presence of recycled materials, the proposed configuration can consistently control the sample Young's modulus to the same level as the benchmark samples (50 % − 50 % new-aged mixed blend).

The total build time for tensile bars without interlayer heating is 35 min (25 min of preheating and 10 min of printing). As a trade-off of successfully reusing extremely aged powders and improved mechanical properties, for the tensile bars with interlayer heating, the interlayer heating time is 10 min (60 s × 10 layers) for a batch. The total build time for tensile bars with interlayer heating is 45 min (25 min of preheating, 10 min of printing and 10 min of interlayer heating). The proposed SLS with interlayer heating aims to provide the needed heating energy to improve part mechanical properties through promoting powder coalescence and part densification. In practice, engineering judgements are recommended to balance material cost, part design, and urgency of the manufacturing task when recycling and reusing the materials.

4. Conclusions

A new process control method was proposed in this paper to explore the possibility and feasibility of reusing the differently degraded polyamide 12 powders in different combinations. In particular, the proposed method successfully reuses extremely aged polyamide 12 powders close to the heat-affected zones. The proposed method is composed of seven steps, including powders sample collection, powder preprocess, powder mixing, powder characterizations, parameter control, SLS with interlayer heating and part characterizations. This method enabled reusing reclaimed polyamide 12 powders in different

situations: only pure powders, new-aged mixed powders, new-extremely aged mixed powders with different mixing percentages and new-aged-extremely aged mixed powders with different mixing percentages.

The proposed method of SLS created parts with improved mechanical properties: the largest tensile strength we obtained is 37.97 Mpa from tensile bars 3D printed using 60 % − 40 % new-extremely aged powders with 60-second interlayer heating, a result 47.17 % better than the baseline (25.80 Mpa). The tensile bars which have stably large elongations at break are from the 10 %–90 % new-extremely aged blends without or with interlayer heating (15.37 % and 16.59 % respectively). Compared to the baseline sample, the tensile bars 3D printed using 30 %–40 %-30 % new-aged-extremely aged mixed powders with 60-second interlayer heating yield 18.04 % higher tensile strength and 55.29 % larger elongation at break.

Declaration of Competing Interest

The authors declare that they have no known competing financial interests or personal relationships that could have appeared to influence the work reported in this paper.

Acknowledgments

The work was supported in part by a research grant from Unilever and by NSF award 1953155.

References

[1] Kruth J-P, Wang X, Laoui T, Froyen L. Lasers and materials in selective laser sintering. Assembly automation. 2003.
[2] Goodridge R, Tuck C, Hague R. Laser sintering of polyamides and other polymers. Prog Mater Sci 2012;57:229–67.
[3] Chen P, Tang M, Zhu W, Yang L, Wen S, Yan C, et al. Systematical mechanism of Polyamide-12 aging and its micro-structural evolution during laser sintering. Polym Test 2018;67:370–9.
[4] Dadbakhsh S, Verbelen L, Verkinderen O, Strobbe D, Van Puyvelde P, Kruth J-P. Effect of PA12 powder reuse on coalescence behaviour and microstructure of SLS parts. Eur Polym J 2017;92:250–62.
[5] Chen B, Wang Y, Berretta S, Ghita O. Poly Aryl Ether Ketones (PAEKs) and carbon-reinforced PAEK powders for laser sintering. J Mater Sci 2017;52:6004–19.
[6] Berretta S, Evans KE, Ghita O. Processability of PEEK, a new polymer for high temperature laser sintering (HT-LS). Eur Polym J 2015;68:243–66.
[7] McAlea K. Materials and applications for the selective laser sintering. Process, Proc. 7th Int. Conf. on Rapid Prototyping 1997:23–33.
[8] Ziegelmeier S, Christou P, Wöllecke F, Tuck C, Goodridge R, Hague R, et al. An experimental study into the effects of bulk and flow behaviour of laser sintering polymer powders on resulting part properties. J Mater Process Technol 2015;215:239–50.
[9] Zarringhalam H, Hopkinson N, Kamperman N, De Vlieger J. Effects of processing on microstructure and properties of SLS Nylon 12. Mater Sci Eng A 2006;435:172–80.
[10] Wang G, Wang P, Zhen Z, Zhang W, Ji J. Preparation of PA12 microspheres with tunable morphology and size for use in SLS processing. Mater Des 2015;87:656–62.
[11] Arai S, Tsunoda S, Kawamura R, Kuboyama K, Ougizawa T. Comparison of crystallization characteristics and mechanical properties of poly (butylene terephthalate) processed by laser sintering and injection molding. Mater Des 2017;113:214–22.
[12] Paolucci F, van Mook M, Govaert L, Peters G. Influence of post-condensation on the crystallization kinetics of PA12: from virgin to reused powder. Polymer 2019;175:161–70.
[13] Schmid M, Amado A, Wegener K. Polymer powders for selective laser sintering (SLS). AIP Conference Proceedings. 2015. pp. 160009.
[14] Feng L, Wang Y, Wei Q. PA12 powder recycled from SLS for FDM. Polymers 2019;11:727.
[15] Dotchev K, Yusoff W. Recycling of polyamide 12 based powders in the laser sintering process. Rapid Prototyp J 2009.
[16] Pham DT, Dotchev K, Yusoff W. Deterioration of polyamide powder properties in the laser sintering process. Proc Inst Mech Eng Part C J Mech Eng Sci 2008;222:2163–76.
[17] Ziegelmeier S, Wöllecke F, Tuck C, Goodridge R, Hague R. Characterizing the bulk & flow behaviour of LS polymer powders. Proceedings SFF Symposium. 2013.
[18] Krantz M, Zhang H, Zhu J. Characterization of powder flow: static and dynamic testing. Powder Technol 2009;194:239–45.
[19] Ligon SC, Liska R, Stampfl Jr, Gurr M, Mülhaupt R. Polymers for 3D printing and customized additive manufacturing. Chem Rev 2017;117:10212–90.
[20] Wegner A, Mielicki C, Grimm T, Gronhoff B, Witt G, Wortberg J. Determination of robust material qualities and processing conditions for laser sintering of polyamide 12. Polym Eng Sci 2014;54:1540–54.
[21] Wang L, Kiziltas A, Mielewski DF, Lee EC, Gardner DJ. Closed-loop recycling of polyamide12 powder from selective laser sintering into sustainable composites. J Clean Prod 2018;195:765–72.
[22] Wudy K, Drummer D. Aging effects of polyamide 12 in selective laser sintering: molecular weight distribution and thermal properties. Addit Manuf 2019;25:1–9.
[23] Wudy K, Drummer D. Aging behavior of polyamide 12: interrelation between bulk characteristics and part properties. Solid Freeform Fabrication Symposium—an Additive Manufacturing Conference 2016:770–81.
[24] Goodridge R, Hague R, Tuck C. Effect of long-term ageing on the tensile properties of a polyamide 12 laser sintering material. Polym Test 2010;29:483–93.
[25] Wudy K, Drummer D, Kühnlein F, Drexler M. Influence of degradation behavior of polyamide 12 powders in laser sintering process on produced parts. AIP Conference Proceedings. 2014. p. 691–5.
[26] Wegner A, Witt G. Correlation of process parameters and part properties in laser sintering using response surface modeling. Phys Procedia 2012;39:480–90.
[27] Pavan M, Faes M, Strobbe D, Van Hooreweder B, Craeghs T, Moens D, et al. On the influence of inter-layer time and energy density on selected critical-to-quality properties of PA12 parts produced via laser sintering. Polym Test 2017;61:386–95.
[28] Hofland EC, Baran I, Wismeijer DA. Correlation of process parameters with mechanical properties of laser sintered PA12 parts. Adv Mater Sci Eng 2017;2017.
[29] Salmoria G, Lauth V, Cardenuto M, Magnago R. Characterization of PA12/PBT specimens prepared by selective laser sintering. Opt Laser Technol 2018;98:92–6.
[30] Schmid M, Kleijnen R, Vetterli M, Wegener K. Influence of the origin of polyamide 12 powder on the laser sintering process and laser sintered parts. Appl Sci 2017;7:462.
[31] Li R, Hu X. Study on discoloration mechanism of polyamide 6 during thermo-oxidative degradation. Polym Degrad Stab 1998;62:523–8.
[32] Gijsman P, Tummers D, Janssen K. Differences and similarities in the thermo-oxidative degradation of polyamide 46 and 66. Polym Degrad Stab 1995;49:121–5.